ACS Chemical Neuroscience pubs.acs.org/acschemicalneuroscience Article

Histone Deacetylase Inhibitor MS-275 Exhibits Poor Brain Penetration: Pharmacokinetic Studies of [^{11}C]MS-275 using Positron Emission Tomography

Jacob M. Hooker,*[,†] Sung Won Kim,[†,‡] David Alexoff,[†] Youwen Xu,[†] Colleen Shea,[†] Alicia Reid,[†,§] Nora Volkow,[†,‡,⊥] and Joanna S. Fowler[†]

[†]Medical Department, Brookhaven National Laboratory, Upton, New York 11973, [‡]National Institute on Alcohol Abuse and Alcoholism, Rockville, Maryland 20892, [§]School of Science, Health and Technology, Medgar Evers College, Brooklyn, New York 11225, and [⊥]National Institute on Drug Abuse, Rockville, Maryland 20892

Abstract

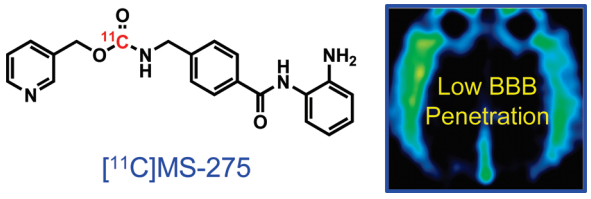

MS-275 (entinostat) is a histone deacetylase (HDAC) inhibitor currently in clinical trials for the treatment of several types of cancer. Recent reports have noted that MS-275 can cross the blood−brain barrier (BBB) and cause region-specific changes in rodent brain histone acetylation. To characterize the pharmacokinetics and distribution of MS-275 in the brain using positron emission tomography (PET), we labeled the carbamate carbon of MS-275 with carbon-11. Using PET, we determined that [^{11}C]MS-275 has low uptake in brain tissue when administered intravenously to nonhuman primates. In rodent studies, we observed that pharmacokinetics and brain accumulation of [^{11}C]MS-275 were not changed by the coadministration of large doses of unlabeled MS-275. These results, which both highlight the poor brain penetration of MS-275, clearly suggest its limitation as a therapeutic agent for the central nervous system (CNS). Moreover, our study demonstrates the effectiveness of PET at providing brain pharmacokinetic data for HDAC inhibitors. These data are important not only for the development of new compounds for peripheral cancer treatment (where CNS exclusion is often advantageous) but also for the treatment of neurological disorders (where CNS penetration is critical).

Keywords: MS-275, entinostat, carbon-11, PET, HDAC, histone deacetylase, epigenetics, brain

Therapeutic agents targeting epigenetic mechanisms have shown promise in the treatment of a broad spectrum of human disease, primary among them being cancer (*1*, *2*). In particular, small-molecule histone deacetylase inhibitors (HDIs) have been pursued extensively for the treatment of malignant tumors due to their ability to suppress cell proliferation (*3*). Identification of the natural product trichostatin A as a potent HDI led medicinal chemists to the hydroxamate class of HDIs that includes suberoylanilide hydroxamic acid (SAHA, marketed as vorinostat, Figure 1), now an approved treatment for cutaneous T cell lymphoma. In parallel to the development of the hydroxamate-based HDI class, a structurally unrelated class of HDIs, benzamide derivatives, was identified (*4*, *5*). Both classes of compounds are believed to bind the zinc cation in the active site of the enzyme but can exhibit preferential binding to certain classes of histone deacetylase (HDAC) isoforms or even members within a class (*6*−*8*). MS-275 (entinostat) is among the benzamide HDIs in phase II clinical development for several types of cancer (*9*).

Although SAHA, MS-275, and other HDIs are being pursued most actively for cancer therapy, there is a growing interest in the use of HDIs for neurological and psychiatric disorders, including (among many others) depression, addiction, schizophrenia, bipolar disorder, Alzheimer's disease, and Huntington's disease (*10*). In fact, there is a long history of antipsychotic treatment with HDIs including most notably the use of valproic acid as a mood stabilizer (*11*). Thus, the application of molecules identified as HDIs for the treatment of cancer to diseases and functions of the brain is an active area of research (*12*−*16*).

Unfortunately, to date very little is known about the concentration and distribution of histone deacetylases (HDACs) in the human brain. The information that is known about the distribution of HDACs comes from mRNA hybridization assays in rodent brain slices (*17*, *18*). While these studies have been able to

Received Date: October 5, 2009
Accepted Date: October 14, 2009

Published on Web Date: October 21, 2009

DOI: 10.1021/cn9000268 | ACS Chem. Neurosci. (2010), 1, 65–73

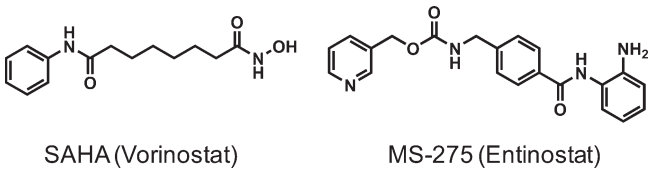

Figure 1. Structures of SAHA and MS-275.

differentiate HDAC isoforms and associate the isoforms with particular brain regions, they do not provide information about the HDAC protein expression levels and activity. In an effort to characterize HDAC levels (and potentially their activity) in the human brain, we have pursued the development of positron emission tomography (PET) ligands based on HDIs (*19*). As part of these efforts, we are also investigating the pharmacokinetics and distribution of drug molecules that are being targeted for HDAC inhibition in the central nervous system (CNS). We anticipate that the combined goals of HDAC radiotracer development and HDI drug characterization by PET will accelerate small-molecule HDIs for the CNS. In this study, we focus on the characterization of MS-275.

MS-275 was reported to be a potent, long-lasting brain region selective inhibitor of HDACs (*20*). Intriguingly, acetylation at histone 3 was dose dependently increased in the rat hippocampus (up to 3-fold) and the frontal cortex (up to 2-fold), but not in other brain regions such as the striatum. The origin of brain region selectivity could be attributed to a number of factors including HDAC isoform distribution differences or MS-275 distribution and pharmacokinetics, but in the absence of further characterization, no conclusions could be drawn as to which was the cause of brain region selectivity (*20*). In addition to this report, other reports have cited the blood−brain barrier (BBB) permeability of MS-275 (*21*, *22*), but all reports to date have relied on the indirect measurement of MS-275 in the brain via changes in histone acetylation.

Our goals were to characterize the BBB penetration of MS-275 and evaluate the pattern of its distribution in the rodent and primate brain *in vivo* with PET. To accomplish this, we developed a method to label MS-275 with the positron emitting isotope carbon-11 ($t_{1/2}$ = 20.4 min). Carbon-11 incorporation at the carbamate carbon of MS-275 was possible due to the recent development of reaction methodology for direct [^{11}C]carbon dioxide fixation (*23*). Herein, we describe the synthesis of [^{11}C]MS-275 and show that BBB penetration of MS-275 is remarkably poor, regardless of administered dose and species.

Results and Discussion

The radiosynthesis of [^{11}C]MS-275 was based on our recent report for direct incorporation of $^{11}CO_2$ into the carbamate carbon (*23*). We have previously shown that among common tertiary amines, 1,8-diazabicyclo-[5.4.0]undec-7-ene (DBU) was effective at both trapping $^{11}CO_2$ and C-11 carbamate formation with an amine and an alkyl halide. In the case of MS-275, the required alkyl chloride (3-picolyl chloride, **4**) was commercially available as the hydrochloride salt. Thus, only the amine portion needed to be prepared. Although the precursor amine (**3**) could be accessed through hydrogenolysis of MS-275, we obtained the amine (**3**) using a straightforward sequence outlined in Figure 2. A sample of MS-275 was prepared as a reference standard according to the literature (*24*).

By using the direct fixation labeling method for carbon-11 incorporation, we were able to avoid protection of the aryl amine of precursor **3**. While both alkyl amines and aryl amines are competent in the $^{11}CO_2$ direct incorporation method, alkyl amines are superior substrates, and we noted exclusive formation of the desired product without competition from the aryl amine. In one pot, a solution of precursors **3** and **4** (both as hydrochloride salts in DMF) were combined with excess DBU. After $^{11}CO_2$ was trapped and the reaction solution was warmed to 75 °C for 7 min, excess $^{11}CO_2$ was removed and [^{11}C]MS-275 was isolated by reversed-phase chromatography. Given the short half-life of carbon-11 (20.4 min), this one-pot, one-step procedure (without protecting groups) was highly effective providing >20 mCi of [^{11}C]MS-275 per synthesis with relative ease. We expect analogous reaction conditions could be used for the preparation of MS-275 containing other carbon isotopes (^{13}C and ^{14}C), which may prove valuable tools in epigenetic research.

With [^{11}C]MS-275 available, we examined its lipophilicity and plasma protein binding *in vitro*. Both the log *D* (1.79 ± 0.08, n = 6) and plasma protein binding (PPB, 7.10% unbound, n = 2) appeared suitable for BBB penetration (*25*). Our data suggested a lower free fraction of MS-275 in plasma than previously reported. However, previous investigations of MS-275 plasma protein binding noted substantial species differences, which may in part explain this difference given our use of the baboon model (*26*). Given the literature precedence and our analysis of the physical properties of MS-275, including its molecular weight, lipophilicity, and PPB character, we fully anticipated good BBB penetration *in vivo*.

Using PET, we determined that [^{11}C]MS-275 exhibited very poor initial BBB penetration and low brain uptake over the scanning time (90 min) when administered intravenously to a baboon, Figure 3. This result was reproduced in two different animals. A concentration of less than 0.001% of the injected dose per cubic centimeter was distributed in the brain tissue. Coregistration of the PET image with an MRI of the same

DOI: 10.1021/cn9000268 | *ACS Chem. Neurosci.* (2010), *1*, 65–73

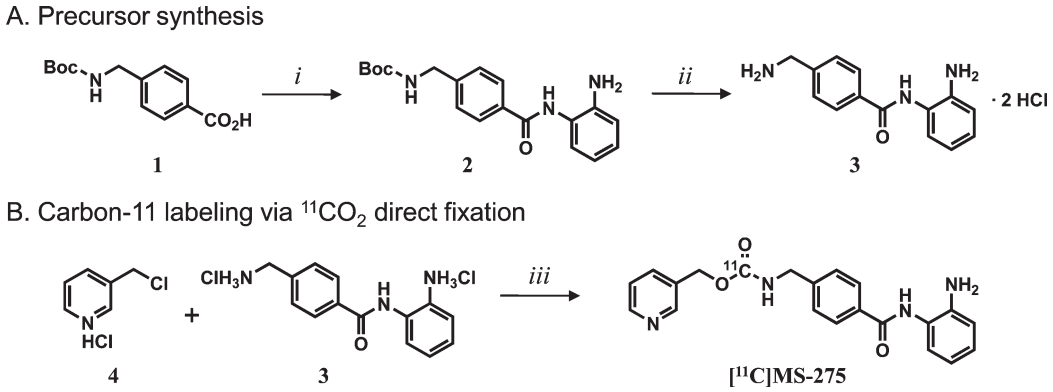

Figure 2. Synthesis of the labeling precursor and [^{11}C]MS-275. Reagents and conditions: (i) CDI, THF, reflux, 3 h, 50%; (ii) TFA, $CHCl_3$, rt, 2 h, 96% then HCl, Et_2O; (iii) $^{11}CO_2$, DBU, DMF, 75 °C, 7 min, 25% RCY.

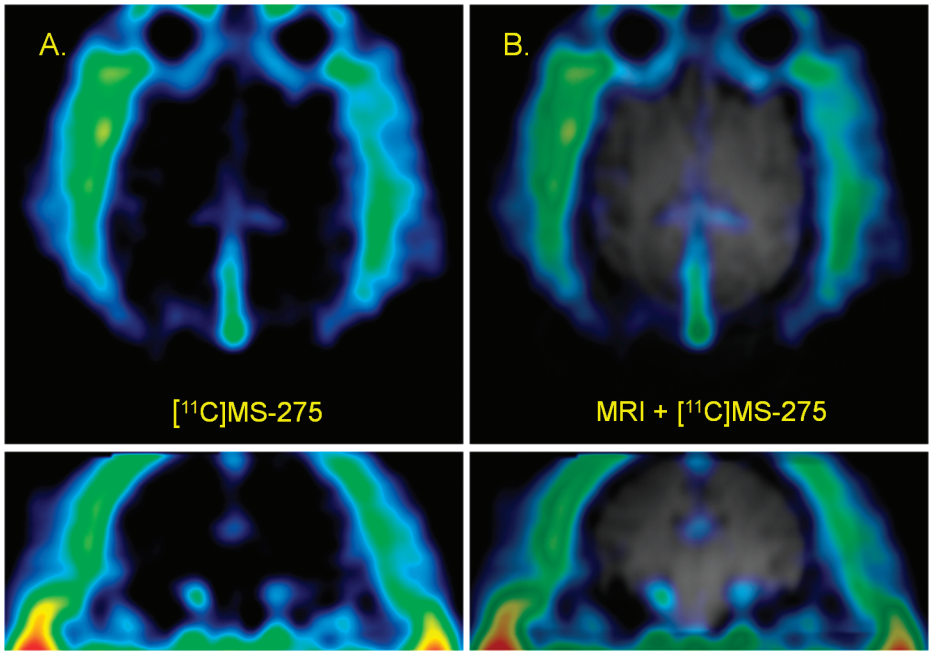

Figure 3. [^{11}C]MS-275 PET Imaging (baboon brain): (a) summed PET images (2−90 min) following injection of [^{11}C]MS-275 (4.85 mCi); (b) PET image superimposed with a structural MRI of the brain from the same baboon.

animal indicated that the areas appearing to have a high level of radioactivity corresponded to the ventricles and are likely outside of the BBB. As an initial probe of the cause of poor BBB uptake, verapamil (0.5 mg/kg iv, 5 min prior to [^{11}C]MS-275) was used to block P-glycoprotein efflux (verapamil is a P-gp substrate that has been used to increase BBB penetration of other compounds; for recent examples, see refs (*27*−*29*)). However, we did not observed a change in [^{11}C]MS-275 BBB permeability and retention nor the overall pharmacokinetics of [^{11}C]MS-275 with verapamil pre-treatment. Although our data suggest that P-gp may not be a major mechanism of MS-275 brain exclusion, further *in vitro* and *in vivo* experiments will be required to rule out P-gp mediated efflux and to determine what other mechanisms are at play.

After [^{11}C]MS-275 was administered intravenously, carbon-11 was cleared from circulation by both the renal and biliary systems. Following a 90 min dynamic PET scan of the brain, [^{11}C]MS-275 and its labeled metabolites were primarily found in the urinary bladder (as determined by a segmented rectilinear scan, data not shown). A dynamic scan of the baboon's torso following [^{11}C]MS-275 administration indicated that in addition to the bladder, radioactivity accumulated in the kidneys, liver, and gallbladder (Figure 4).

Arterial plasma samples were collected during each of the four PET scans, and the percentage of carbon-11 associated with [^{11}C]MS-275 was determined using HPLC, Figure 5. After 40 min, approximately 60% of the radioactivity in plasma was still associated with [^{11}C]MS-275. Given orally, MS-275 was reported to

DOI: 10.1021/cn9000268 | *ACS Chem. Neurosci.* (2010), *1*, 65–73

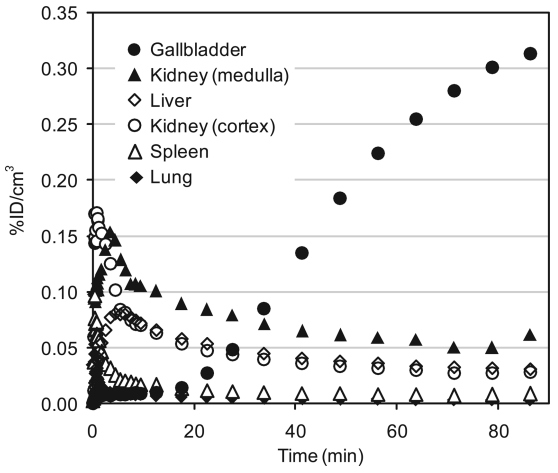

Figure 4. Time−activity curves derived from PET imaging data for peripheral organs in the baboon torso following administration of [^{11}C]MS-275 (4.74 mCi).

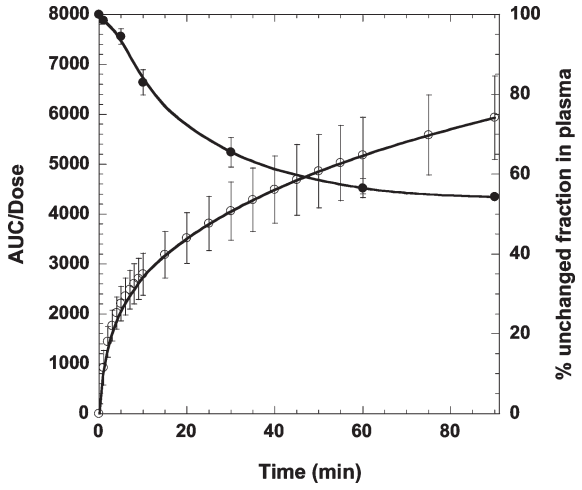

Figure 5. Baboon plasma analysis: (●) percentage (of total radioactivity) of [^{11}C]MS-275 in plasma over time; (○) metabolite-corrected plasma integral.

have good metabolic stability and a long circulation half-life (mean terminal half-life, 33.9 ± 26.2 h) (*30*). However, both dose and frequency of administration affect the circulation half-life (52−150 h) (*31*). Our study provides rate data for initial clearance at much earlier time points than previous studies and is consistent with rapid initial clearance previously observed. The persistence of unmetabolized MS-275 at later time points (>60 min), as well as the continuing rise of the plasma integral (AUC) over time, is also consistent with the previous pharmacokinetic data reported (*30*, *31*).

Given that [^{11}C]MS-275 exhibited poor BBB penetration in baboon and that several reports have cited the ability of MS-275 to cross the BBB in rodents (*20*−*22*), we became interested in determining whether species or dose effects or both existed for MS-275 entry and accumulation in the brain. Using small animal PET imaging, we evaluated the pharmacokinetics of [^{11}C]MS-275 (adminstered iv) in the rat brain before and after administration of MS-275 (40 mg/kg ip), Figure 6. As with the baboon, [^{11}C]MS-275 showed very little BBB penetration and brain accumulation (<0.10% ID/cm^3 after only 3 min). The pharmacokinetics of [^{11}C]MS-275 were not affected by the administration of a large dose of cold (i.e., nonlabeled) MS-275. It is important to note that the clinical dose of MS-275 (6 mg/m^2 po) used to treat solid tumors and lymphomas is *at least 2 orders of magnitude lower* than the doses used in previous reports of MS-275 brain penetration and CNS effects and in this study.

To further investigate the effect of MS-275 dose on BBB penetration, we coadministered [^{11}C]MS-275 and MS-275 to mice subcutaneously. Our choice of dose, route of administration, and tissue sampling time was based on the work by Simonini et al. (*20*), which demonstrated that MS-275 altered histone acetylation in several of brain regions. We administered nominally

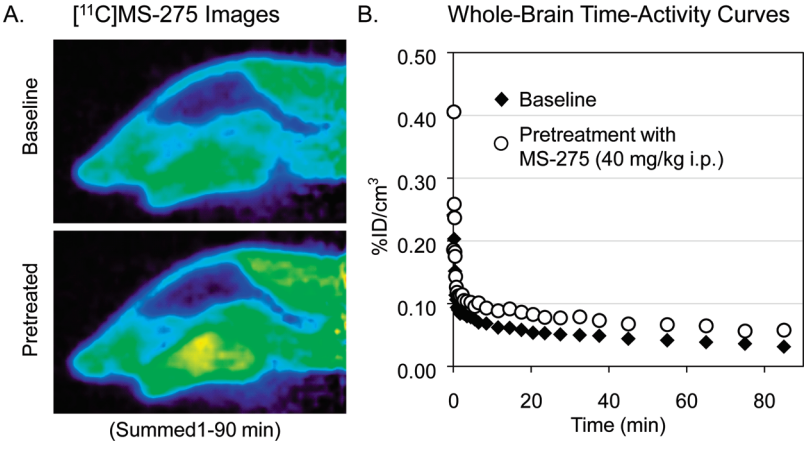

Figure 6. Rodent imaging experiments with [^{11}C]MS-275. (a) Summed PET images (1−90 min) following injection of [^{11}C]MS-275: (top) baseline scan (1.74 mCi); (bottom) image acquired following pretreatment with MS-275 (40 mg/kg ip; 1.39 mCi). Images are dose corrected. (b) Whole-brain time−activity curves generated from imaging data.

DOI: 10.1021/cn9000268 | *ACS Chem. Neurosci.* (2010), *1*, 65–73

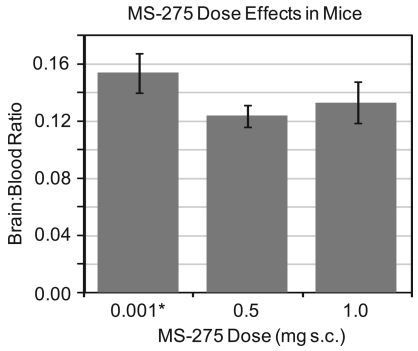

Figure 7. Ratio of radioactivity in brain and blood (at 2 h) for mice coadministered [^{11}C]MS-275 with nonradioactive MS-275 at two doses: ∗ indicates injection of [^{11}C]MS-275 only.

1.0 mCi of [^{11}C]MS-275 alone or with either 0.5 mg or 1.0 mg of MS-275 (all animals were 22 ± 1 g). This very high dose corresponds to approximately 0, 25, and 50 mg/kg (0, 60, 120 μmol/kg). We sacrificed each animal 2 h after the injection and determined the amount of radioactivity in blood and brain, Figure 7. We did not observe a change in the ratio of radioactivity in the brain to blood as a function of dose. The ratio for each dose was ∼0.12−0.15, again demonstrating the poor BBB penetration of MS-275. Metabolite analysis of brain homogenate from two animals (one administered [^{11}C]MS-275 only and one coadministered with 1.0 mg MS-275) indicated that 80% of the radioactivity in the brain was associated with [^{11}C]MS-275.

Although the brain/blood ratio was consistent from one animal to another, the overall amount of radioactivity that accumulated in the brain varied greatly from animal to animal (even within a group given a particular dose). Using the absolute amount of radioactivity in the brain and the known mass injected, we determined the mass of MS-275 in the brain at 2 h for each given dose. At 60 μmol/kg, there was 326 ± 105 ng of MS-275 per gram of brain tissue at 2 h. At 120 μmol/kg, there was 709 ± 312 ng of MS-275 per gram of brain tissue at 2 h. This calculation assumes that all of the radioactivity in the brain is [^{11}C]MS-275 and is therefore an *upper limit* measurement of the actual value.

We surmise that although MS-275 BBB penetration is very poor at high doses such as those used by Simonini et al. (*20*), sufficient quantities may reside in the brain for the HDAC inhibition observed. However, at the doses of MS-275 used clinically, it is unlikely that a high enough concentration of MS-275 enters the brain to alter histone acetylation (at least acutely). The effect of chronic MS-275 administration at low doses on histone acetylation in the brain will require further investigation.

Conclusions

The histone deacetylase inhibitor, MS-275, was labeled with carbon-11 by the direct incorporation of $^{11}CO_2$. Using PET, we determined that MS-275 exhibits poor initial BBB penetration and accumulation regardless of species and dose administered. The low BBB penetration and accumulation of MS-275 is perhaps a good attribute given its use as a HDAC inhibitor for the treatment of peripheral cancer, where the low BBB penetration and relatively low clinical doses of MS-275 will undoubtedly minimize unwanted CNS effects. Although we note poor BBB penetration of MS-275, this does not necessarily exclude it as a candidate for gliomas in which the BBB may be compromised, allowing penetration. Our studies suggest that the efficacy of MS-275 for the treatment of neurological disorders by targeting HDACs in the CNS will not be good and that new HDAC inhibitors designed specifically for the CNS are urgently needed.

Methods

General

[^{11}C]Carbon dioxide was generated from a nitrogen/oxygen (1000 ppm) target (^{14}N(p,α)^{11}C) using an EBCO TR 19 cyclotron (Advanced Cyclotron Systems INC. Richmond, Canada). High-performance liquid chromatography (HPLC) purification was performed by a Knauer HPLC system (Sonntek Inc., Woodcliff Lake, NJ) with a model K-5000 pump, a Rheodyne 7125 injector, a model 87 variable wavelength monitor, and a NaI radioactivity detector.

Specific activity was determined by measuring the radioactivity and the mass; the latter was derived from a standard curve (UV absorbance at 254 nm by peak area) after HPLC injection of different quantities of the authentic reference compound. Radiochemical purity was determined by HPLC and verified by thin-layer chromatography (TLC) using and measuring radioactivity distribution on Macherey−Nagel polygram sil G/UV254 plastic-backed TLC plates with a Bioscan system 200 imaging scanner (Bioscan Inc., Washington, DC). ^{11}C-Radioactivity was measured by a MINAXI γ 5000 automated gamma counter (Packard Instrument, Meriden, CT). All measurements were decay corrected. Mass spectra were recorded on a Thermo Finnigan LCQ Advantage. All chemicals were purchased from Sigma-Aldrich, with the exception of anhydrous DMF, which was obtained from Acros Organics.

MS-275 Synthesis. MS-275 synthesis was accomplished by a published method (*24*).

MS-275 Precursor Synthesis

4-(Boc-aminomethyl)-*N*-(2-aminophenyl)benzamide (2). Into a suspension of 4-(Boc-aminomethyl)benzoic acid (170 mg, 0.68 mmol) in anhydrous tetrahydrofuran (THF, 4 mL) was added 1,1′-carbonyldiimidazole (124.8 mg, 0.77 mmol) at room temperature. The mixture was heated to reflux for 3 h. The resulting clear solution was added dropwise into a mixture of 1,2-phenylenediamine (110.3 mg, 1.00 mmol) and 4-dimethylaminopyridine (DMAP, 16 mg, 0.13 mmol) in THF (10 mL) at 40 °C. After the mixture was stirred for 2 h, the solvent was removed. The residue was triturated with water and filtered to give a yellowish solid

DOI: 10.1021/cn9000268 | *ACS Chem. Neurosci.* (2010), *1*, 65–73

(116 mg, 50%) and used without further purification. ^{1}H NMR (400 MHz, CD_3OD): δ (ppm) 1.47 (s, 9H), 4.31 (s, 2H), 6.78 (t, 1H), 6.91 (d, 1H), 7.08 (t, 1H), 7.19 (d, 1H), 7.42 (d, 2H), 7.94 (d, 1H). ^{13}C NMR (400 MHz, CD_3OD): δ (ppm) 28.90, 44.84, 80.48, 118.92, 119.87, 125.51, 127.79, 128.32, 128.69, 129.16, 134.33, 143.88, 145.50, 158.75, 168.85. ESI-MS calcd $[M + H]^+$ 342.2, found 342.1.

4-(Aminomethyl)-*N*-(2-aminophenyl)benzamide·2HCl (3). Into a mixture of trifluoroacetic acid (TFA, 1 mL) and chloroform (1 mL) was added the Boc-protected benzamide **2** (100 mg, 0.30 mmol). After the mixture was stirred for 2 h, TFA and chloroform were removed under reduced pressure. The residue was dissolved with ethyl acetate and washed with an aqueous solution of sodium hydroxide (0.1%), then water, and finally a solution of saturated sodium chloride (aq). The ethyl acetate layer was dried over anhydrous sodium sulfate, filtered, and evaporated to dryness affording a slightly yellow solid (69.5 mg, yield 96%). ^{1}H NMR (400 MHz, CD_3OD): δ (ppm) 3.88 (s, 2H), 6.78 (t, 1H), 6.91 (d, 1H), 7.09(t, 1H), 7.19 (d, 1H), 7.49 (d, 2H), 7.96 (d, 1H). ^{13}C NMR (400 MHz, CD_3OD): δ (ppm) 46.48, 118.93, 119.87, 125.52, 127.79, 128.68, 129.24, 134.16, 143.91, 148.05, 168.85. ESI-MS calcd $[M + H]^+$ 242.1, found 242.1. The free amine was converted into a salt form with hydrogen chloride in ether (1.0 M) for storage. The HCl salt of **3** was used as the precursor for carbon-11 radiolabeling.

Radiosynthesis of [^{11}C]MS-275

Atmospheric carbon dioxide in two DMF solutions (DBU in DMF (1.0 M) and 3-picoyl chloride hydrochloride (0.30 M)) was removed by sparging the solutions with a stream of ultrapure helium gas for 30 min. Into a V-shape vial with septum-sealed cap containing 4-(aminomethyl)-*N*-(2-aminophenyl)benzamide·2HCl (2.0 mg) was added an aliquot (100 μL) of each DMF solution. The combined contents were mixed by vortex and then sparged with helium gas for at least 10 min. At the end of bombardment (EOB), [^{11}C]carbon dioxide from the target gases was trapped on crushed molecular sieves then released into a helium stream (~75 mL/min) by heating the molecular sieves to 250 °C. The trapping and releasing allowed a bolus of $^{11}CO_2$ to be delivered to the reaction vessel with a lower volume of carrier gas. The gaseous radioactivity was transferred into the reaction solution until radioactivity in the vessel reached a maximum (as observed by a miniature pin-diode detector in proximity to the vessel). Trapping efficiencies for both steps were typically greater than 95%. After introduction of $^{11}CO_2$, the vessel was sealed and heated to 75 °C for 7 min, at which time the heating bath was removed and He gas was used to sparge out remaining (unreacted $^{11}CO_2$). The reaction mixture was acidified with formic acid (0.1 mL) to ensure the total residual [^{11}C]carbon dioxide was removed and sparging with He continued. Typically, 30% of the radioactivity remained in the vessel as estimated by the proximal radioactivity detector. After dilution with HPLC eluent (1.0 mL), [^{11}C]MS-275 was purified on a Luna C18(2) column (250 × 10 mm^2, 5 μm particles) using an isocratic solvent system (5 mL/min, 80% (0.1 M (aq) ammonium formate)/20% MeCN). The fraction containing [^{11}C]MS-275 was collected (retention time 19−20 min), and the solvent was removed on a rotary evaporator. Following purification and concentration, [^{11}C]MS-275 was dissolved in saline (4.0 mL), and the resulting solution was filtered through an Acrodisc 13-mm syringe filter with 0.2 μm HT Tuffryn Membrane (Pall Corporation, Ann Arbor, MI) into a sterile vial for delivery to the imaging facility. The radiochemical yield based on the loss of volatile $^{11}CO_2$ and HPLC was typically 25% (decay corrected to EOB). Specific activity for the imaging studies was 2.7−6.2 Ci/μmol (calculated at EOB). Typical radiosynthesis and purification time was 50 min.

For quality control (i.e., identity verification and radiochemical purity), analytical TLC and HPLC were performed. [^{11}C]MS-275 was cospotted with unlabeled (i.e., non-radioactive) standard and analyzed by radioTLC (EtOAc with 0.1% TEA, R_f = 0.6). Analytical HPLC was accomplished using a Phenomenex Gemini C18 column (250 × 4.6 mm^2, 5 μm particles) using a gradient elution (1.0 mL/min) from a 95% aqueous mobile phase to 5% aqueous (balance MeCN) over 20 min. By this method, [^{11}C]MS-275 eluted at 17.2 min. Radiochemical purity exceeded 98% as determined by both radioHPLC and radioTLC, and chemical purity was >95% as determined from analytical HPLC.

log *D* Determination

An aliquot (~50 μL) of the formulated [^{11}C]MS-275 was added to a test tube containing 2.5 mL of octanol and 2.5 mL of phosphate buffer solution (pH 7.4). The test tube was mixed by vortex for 2 min and then centrifuged for 2 min to fully separate the aqueous and organic phase. A sample taken from the octanol layer (0.1 mL) and the aqueous layer (1.0 mL) was saved for radioactivity measurement. An additional aliquot of the octanol layer (2.0 mL) was carefully transferred to a new test tube containing 0.5 mL of octanol and 2.5 mL of phosphate buffer solution (pH 7.4). The previous procedure (vortex mixing, centrifugation, sampling, and transfer to the next test tube) was repeated until six sets of aliquot samples had been prepared. The radioactivity of each sample was measured in a well counter (Picker, Cleveland, OH). The log *D* of each set of samples was derived by the following equation: log *D* = log(decay-corrected radioactivity in octanol sample × 10/decay-corrected radioactivity in phosphate buffer sample).

Plasma Protein Binding Assay

An aliquot of [^{11}C]MS-275 in saline (10 μL) was added to a sample of baboon plasma (0.8 mL, pooled from at least four separate animals). The mixture was gently mixed by repeated inversion and incubated for 10 min at room temperature. Following incubation a small sample (20 μL) was removed to determine the total radioactivity in the plasma sample (A_T; $A_T = A_{bound} + A_{unbound}$). An additional 0.2 mL of the plasma sample was placed in the upper compartment of a Centrifree tube (Amicon, Inc., Beverly, MA) and then centrifuged for 10 min. The upper part of the Centrifree tube was discarded, and an aliquot (20 μL) from the bottom part of the tube was removed to determine the amount of radioactivity that passed through the membrane ($A_{unbound}$). Plasma protein binding was derived by the following equation: % unbound = $A_{unbound} \times 100/A_T$.

PET Imaging and Arterial Plasma Analysis (Baboon)

All experiments with animals were approved by the Brookhaven Institutional Animal Care and Use Committee.

DOI: 10.1021/cn9000268 | ACS Chem. Neurosci. (2010), 1, 65–73

Two female *Papio anubis* baboons were used for this study. Anesthesia was accomplished by an intramuscular injection of ketamine hydrochloride (10 mg/kg) and then maintained with oxygen (800 mL/min), nitrous oxide (1500 mL/min), and isoflurane (Forane, 1−4%) during scanning. [^{11}C]MS-275 was injected through a catheter placed in a radial arm vein, and arterial blood was sampled through a catheter in the popliteal artery at the following time intervals: every 5 s for 2 min, then at 2, 5, 10, 20, 30, 45, and 60 min. Heart rate, respiration rate, pO_2, and body temperature were checked during the PET scanning. Dynamic PET imaging was performed by Siemens HR+ (Siemens high-resolution, whole-body PET scanner with $4.5 \times 4.5 \times 4.8$ mm^3 resolution at the center of field of view) with the brain in the field of view, for a total of 60 min with the following time frames in 3D mode: 1×10 s, 12×5 s, 1×20 s, 1×30 s, 8×60 s, 4×300 s, 8×450 s. Prior to each emission scan, a transmission scan was obtained by rotating a ^{68}Ge rod source to correct for attenuation. A total of five studies in the baboon were conducted (three of brain, one of torso kinetics, one rectilinear following dynamic brain scan), with an average injected dose of 4.92 ± 0.23 mCi. For one study (brain), verapamil (0.5 mg/kg iv) was administered 5 min prior to the injection of [^{11}C]MS-275.

The percent unmetabolized radiotracer in the baboon's plasma was determined using the following protocol: Baboon plasma (~0.2 mL) sampled at various time points during the PET study was counted and added to a solution of unlabeled standard (20 μL of a 1 mg/mL solution) in acetonitrile (0.3 mL), and the resulting mixture was vortexed and centrifuged. The supernatant was mixed with 0.3 mL of water and then analyzed by HPLC (Waters Bondapak C18 column, 300×3.9 mm^2, 10 μm particles, 70:30 25 mM phosphate buffer pH 7.2/MeCN, 1.2 mL/min) using UV (254 nm) and radioactivity detection. The fraction of radioactivity coeluting with the unlabeled standard relative to the total radioactivity from the HPLC column was measured as the percent of unmetabolized parent compound. The percent recovered from the HPLC during each analysis ranged from 85% to 103%. In addition, percent unmetabolized [^{11}C]MS-275 was determined using CN-E Varian BondElut cartridges (500 mg) and a laboratory robot (*32*). Plasma samples were applied to the solid phase extraction cartridge after dilution in 5 mL of water and measurement of the plasma radioactivity. The cartridge was washed twice with 5 mL of water and twice with 5 mL of 1:1 H_2O/MeOH. The radioactivity remaining on the cartridge was [^{11}C]MS-275 (validated by HPLC). The decay corrected ratio of the radioactivity on the BondElute Cartridge to the initial plasma sample radioactivity was calculated. Recoveries using the robot method were >90%. The averaged data from these two methods is presented in Figure 5.

PET Imaging and Dose Effects (Kinetics) in the Rat Brain

One male Sprague−Dawley rat (248 g, 7−8 weeks old, Taconic Farms) was anesthetized and maintained with isoflurane/oxygen and positioned within a microPET R4 scanner (Siemens Preclinical Imaging System, formerly Concord Microsystems). A tail vein catheter was inserted and flushed with saline and subsequently used for administration of [^{11}C]MS-275. During the first study (baseline), the rodent was administered 1.74 mCi (0.6 mL saline) of [^{11}C]MS-275, and dynamic data were collected in list mode for 90 min. Following this study, anesthesia was maintained and the animal was treated with 40 mg/kg MS-275 (ip, formulated in 1.0 mL of water/acetic acid, pH 5.0). After 10 min, 1.39 mCi (0.5 mL in saline) of [^{11}C]MS-275 was administered, and the animal was scanned for 90 min.

Image Analysis

Emission data from the dynamic scans (PET) were corrected for attenuation and reconstructed using filtered back projection. Emission data for rodent experiments were scatter-corrected and reconstructed without attenuation correction. Regions of interest (ROIs) on the baboon and rodent brain were drawn on summed images and then projected to the dynamic images to obtain time−activity curves (TACs) expressed as %injected dose/cm^3 (decay corrected) versus time.

Effect of Dose on MS-275 BBB Penetration in Mice

Eight adult male Swiss albino mice (Taconic Farms), 21−23 g of body weight, were used for these experiments. Animals were injected subcutaneously with a mixture of nominally 1.0 mCi of [^{11}C]MS-275 spiked into a solution of MS-275 (either vehicle, 0.5 mg, or 1.0 mg) in 225 μL of water/acetic acid adjusted to pH 6.0 with a solution of NaOH. Two animals served as a radiotracer control ([^{11}C]MS-275 only), three animals were treated with 0.5 mg of MS-275 plus [^{11}C]MS-275, and three animals were treated with 1.0 mg of MS-275 plus [^{11}C]MS-275. Following injection, the animals were returned to their home cages and sacrificed after 2 h. Torso blood was collected, and the brain of each animal was removed in order to determine the amount of radioactivity (per gram) in each. The ratio of these two numbers is reported. Two of the brain samples (one control and one high dose) were homogenized with 0.3 mL of water. An aliquot of this mixture (100 μL) was diluted to 0.3 mL with cold (4 °C) acetonitrile causing precipitation and phase separation. The sample was mixed by vortex for 1 min and then separated by centrifugation (2000 rcf, 2 min). The supernatant was spiked with the appropriate standard, and the radioactivity of the sample was measured by γ-counting. The sample was analyzed by HPLC, and the fraction coeluting with the standard was collected. The radioactivity of the collected product was measured. The decay corrected ratio of collected product to initial radioactivity in the homogenate sample was determined.

Author Information

Corresponding Author

*To whom correspondence may be addressed. E-mail: hooker@bnl.gov. Fax: (631) 344-5815.

Funding Sources

This work was carried out at Brookhaven National Laboratory under contract DE-AC02-98CH10886 with the U.S. Department of Energy, supported by its Office of Biological and Environmental Research. J.M.H. was supported by an NIH Postdoctoral Fellowship (Grant 1F32EB008320-01) and through the Goldhaber Distinguished Fellowship program at BNL.

DOI: 10.1021/cn9000268 | *ACS Chem. Neurosci.* (2010), *1*, 65–73

Acknowledgment

The authors are grateful to Dr. Michael Schueller for cyclotron operation, Dr. Stephen Dewey for technical assistance with rodent experiments, and the PET imaging team at BNL (Pauline Carter, Payton King, and Don Warner) for carrying out primate imaging experiments.

References

1. Minucci, S., and Pelicci, P. G. (2006) Histone deacetylase inhibitors and the promise of epigenetic (and more) treatments for cancer. *Nat. Rev. Cancer 6*, 38–51.

2. Papait, R., Monti, E., and Bonapace, I. M. (2009) Novel approaches on epigenetics. *Curr. Opin. Drug Discovery Dev. 12*, 264–275.

3. Acharya, M. R., Sparreboom, A., Venitz, J., and Figg, W. D. (2005) Rational development of histone deacetylase inhibitors as anticancer agents: a review. *Mol. Pharmacol. 68*, 917–932.

4. Saito, A., Yamashita, T., Mariko, Y., Nosaka, Y., Tsuchiya, K., Ando, T., Suzuki, T., Tsuruo, T., and Nakanishi, O. (1999) A synthetic inhibitor of histone deacetylase, MS-27-275, with marked in vivo antitumor activity against human tumors. *Proc. Natl. Acad. Sci. U.S.A. 96*, 4592–4597.

5. Suzuki, T., Ando, T., Tsuchiya, K., Fukazawa, N., Saito, A., Mariko, Y., Yamashita, T., and Nakanishi, O. (1999) Synthesis and histone deacetylase inhibitory activity of new benzamide derivatives. *J. Med. Chem. 42*, 3001–3003.

6. Chen, Y. D., Jiang, Y. J., Zhou, J. W., Yu, Q. S., and You, Q. D. (2008) Identification of ligand features essential for HDACs inhibitors by pharmacophore modeling. *J. Mol. Graphics Model. 26*, 1160–1168.

7. Vannini, A., Volpari, C., Filocamo, G., Casavola, E. C., Brunetti, M., Renzoni, D., Chakravarty, P., Paolini, C., De Francesco, R., Gallinari, P., Steinkuhler, C., and Di Marco, S. (2004) Crystal structure of a eukaryotic zinc-dependent histone deacetylase, human HDAC8, complexed with a hydroxamic acid inhibitor. *Proc. Natl. Acad. Sci. U.S.A. 101*, 15064–15069.

8. Khan, N., Jeffers, M., Kumar, S., Hackett, C., Boldog, F., Khramtsov, N., Qian, X., Mills, E., Berghs, S. C., Carey, N., Finn, P. W., Collins, L. S., Tumber, A., Ritchie, J. W., Jensen, P. B., Lichenstein, H. S., and Sehested, M. (2008) Determination of the class and isoform selectivity of small-molecule histone deacetylase inhibitors. *Biochem. J. 409*, 581–589.

9. Hauschild, A., Trefzer, U., Garbe, C., Kaehler, K. C., Ugurel, S., Kiecker, F., Eigentler, T., Krissel, H., Schott, A., and Schadendorf, D. (2008) Multicenter phase II trial of the histone deacetylase inhibitor pyridylmethyl-N-{4-[(2-aminophenyl)-carbamoyl]-benzyl}-carbamate in pretreated metastatic melanoma. *Melanoma Res. 18*, 274–278.

10. Kazantsev, A. G., and Thompson, L. M. (2008) Therapeutic application of histone deacetylase inhibitors for central nervous system disorders. *Nat. Rev. Drug Discovery 7*, 854–868.

11. Thomas, E. A. (2009) Focal nature of neurological disorders necessitates isotype-selective histone deacetylase (HDAC) inhibitors. *Mol. Neurobiol. 40*, 33–45.

12. Guan, J. S., Haggarty, S. J., Giacometti, E., Dannenberg, J. H., Joseph, N., Gao, J., Nieland, T. J., Zhou, Y., Wang, X., Mazitschek, R., Bradner, J. E., DePinho, R. A., Jaenisch, R., and Tsai, L. H. (2009) HDAC2 negatively regulates memory formation and synaptic plasticity. *Nature 459*, 55–60.

13. Stefanko, D. P., Barrett, R. M., Ly, A. R., Reolon, G. K., and Wood, M. A. (2009) Modulation of long-term memory for object recognition via HDAC inhibition. *Proc. Natl. Acad. Sci. U.S.A. 106*, 9447–9452.

14. Hahnen, E., Eyupoglu, I. Y., Brichta, L., Haastert, K., Trankle, C., Siebzehnrubl, F. A., Riessland, M., Holker, I., Claus, P., Romstock, J., Buslei, R., Wirth, B., and Blumcke, I. (2006) In vitro and ex vivo evaluation of second-generation histone deacetylase inhibitors for the treatment of spinal muscular atrophy. *J. Neurochem. 98*, 193–202.

15. Siebzehnrubl, F. A., Buslei, R., Eyupoglu, I. Y., Seufert, S., Hahnen, E., and Blumcke, I. (2007) Histone deacetylase inhibitors increase neuronal differentiation in adult forebrain precursor cells. *Exp. Brain Res. 176*, 672–678.

16. Gavin, D. P., Rosen, C., Chase, K., Grayson, D. R., Tun, N., and Sharma, R. P. (2009) Dimethylated lysine 9 of histone 3 is elevated in schizophrenia and exhibits a divergent response to histone deacetylase inhibitors in lymphocyte cultures. *J. Psychiatry Neurosci. 34*, 232–237.

17. Broide, R. S., Redwine, J. M., Aftahi, N., Young, W., Bloom, F. E., and Winrow, C. J. (2007) Distribution of histone deacetylases 1−11 in the rat brain. *J. Mol. Neurosci. 31*, 47–58.

18. Allen Brain Atlas: http://www.allenbrainatlas.com.

19. Reid, A. E., Hooker, J., Shumay, E., Logan, J., Shea, C., Kim, S. W., Collins, S., Xu, Y., Volkow, N., and Fowler, J. S. (2009) Evaluation of 6-([^{18}F]fluoroacetamido)-1-hexanoicanilide for PET imaging of histone deacetylase in the baboon brain. *Nucl. Med. Biol. 36*, 247–258.

20. Simonini, M. V., Camargo, L. M., Dong, E., Maloku, E., Veldic, M., Costa, E., and Guidotti, A. (2006) The benzamide MS-275 is a potent, long-lasting brain region-selective inhibitor of histone deacetylases. *Proc. Natl. Acad. Sci. U.S.A. 103*, 1587–1592.

21. Eyupoglu, I. Y., Hahnen, E., Trankle, C., Savaskan, N. E., Siebzehnrubl, F. A., Buslei, R., Lemke, D., Wick, W., Fahlbusch, R., and Blumcke, I. (2006) Experimental therapy of malignant gliomas using the inhibitor of histone deacetylase MS-275. *Mol. Cancer Ther. 5*, 1248–1255.

22. Holsken, A., Eyupoglu, I. Y., Lueders, M., Trankle, C., Dieckmann, D., Buslei, R., Hahnen, E., Blumcke, I., and Siebzehnrubl, F. A. (2006) Ex vivo therapy of malignant melanomas transplanted into organotypic brain slice cultures using inhibitors of histone deacetylases. *Acta Neuropathol. 112*, 205–215.

23. Hooker, J. M., Reibel, A. T., Hill, S. M., Schueller, M. J., and Fowler, J. S. (2009) One-pot, direct incorporation of [^{11}C]CO2 into carbamates. *Angew. Chem., Int. Ed. 48*, 3482–3485.

24. Gediya, L. K., Belosay, A., Khandelwal, A., Purushottamachar, P., and Njar, V. C. (2008) Improved synthesis of histone deacetylase inhibitors (HDIs) (MS-275 and CI-994)

DOI: 10.1021/cn9000268 | *ACS Chem. Neurosci.* (2010), *1*, 65–73

and inhibitory effects of HDIs alone or in combination with RAMBAs or retinoids on growth of human LNCaP prostate cancer cells and tumor xenografts. *Bioorg. Med. Chem. 16*, 3352–3360.

25. Dischino, D. D., Welch, M. J., Kilbourn, M. R., and Raichle, M. E. (1983) Relationship between lipophilicity and brain extraction of C-11-labeled radiopharmaceuticals. *J. Nucl. Med. 24*, 1030–1038.

26. Acharya, M. R., Sparreboom, A., Sausville, E. A., Conley, B. A., Doroshow, J. H., Venitz, J., and Figg, W. D. (2006) Interspecies differences in plasma protein binding of MS-275, a novel histone deacetylase inhibitor. *Cancer Chemother. Pharmacol. 57*, 275–281.

27. Chen, X., Zhou, Z. W., Xue, C. C., Li, X. X., and Zhou, S. F. (2007) Role of P-glycoprotein in restricting the brain penetration of tanshinone IIA, a major active constituent from the root of *Salvia miltiorrhiza* Bunge, across the blood-brain barrier. *Xenobiotica 37*, 635–678.

28. Yu, X. Y., Lin, S. G., Zhou, Z. W., Chen, X., Liang, J., Yu, X. Q., Chowbay, B., Wen, J. Y., Duan, W., Chan, E., Li, X. T., Cao, J., Li, C. G., Xue, C. C., and Zhou, S. F. (2007) Role of P-glycoprotein in limiting the brain penetration of glabridin, an active isoflavan from the root of *Glycyrrhiza glabra*. *Pharm. Res. 24*, 1668–1690.

29. Ejsing, T. B., Hasselstrom, J., and Linnet, K. (2006) The influence of P-glycoprotein on cerebral and hepatic concentrations of nortriptyline and its metabolites. *Drug Metabol. Drug Interact. 21*, 139–162.

30. Kummar, S., Gutierrez, M., Gardner, E. R., Donovan, E., Hwang, K., Chung, E. J., Lee, M. J., Maynard, K., Kalnitskiy, M., Chen, A., Melillo, G., Ryan, Q. C., Conley, B., Figg, W. D., Trepel, J. B., Zwiebel, J., Doroshow, J. H., and Murgo, A. J. (2007) Phase I trial of MS-275, a histone deacetylase inhibitor, administered weekly in refractory solid tumors and lymphoid malignancies. *Clin. Cancer Res. 13*, 5411–5417.

31. Gore, L., Rothenberg, M. L., O'Bryant, C. L., Schultz, M. K., Sandler, A. B., Coffin, D., McCoy, C., Schott, A., Scholz, C., and Eckhardt, S. G. (2008) A phase I and pharmacokinetic study of the oral histone deacetylase inhibitor, MS-275, in patients with refractory solid tumors and lymphomas. *Clin. Cancer Res. 14*, 4517–4525.

32. Alexoff, D. L., Shea, C., Fowler, J. S., King, P., Gatley, S. J., Schlyer, D. J., and Wolf, A. P. (1995) Plasma input function determination for PET using a commercial laboratory robot. *Nucl. Med. Biol. 22*, 893–904.

DOI: 10.1021/cn9000268 | *ACS Chem. Neurosci.* (2010), *1*, 65–73